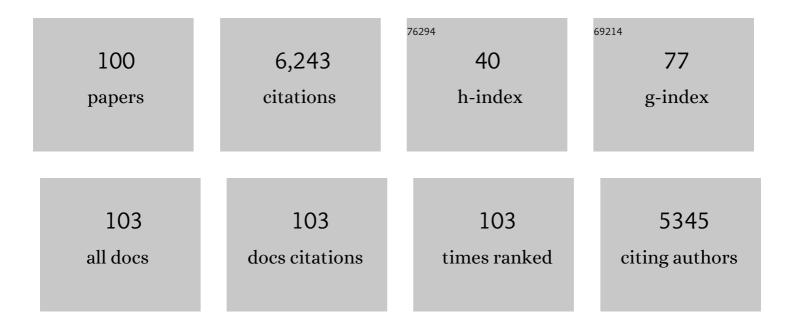
Pyuck-Pa Choi

List of Publications by Year in descending order

Source: https://exaly.com/author-pdf/2356167/publications.pdf Version: 2024-02-01



DVIICK-DA CHOI

#	Article	IF	CITATIONS
1	Grain boundary segregation engineering in metallic alloys: A pathway to the design of interfaces. Current Opinion in Solid State and Materials Science, 2014, 18, 253-261.	5.6	466
2	Atomic-Scale Quantification of Grain Boundary Segregation in Nanocrystalline Material. Physical Review Letters, 2014, 112, 126103.	2.9	284
3	Strain hardening by dynamic slip band refinement in a high-Mn lightweight steel. Acta Materialia, 2016, 116, 188-199.	3.8	276
4	Atomic-scale mechanisms of deformation-induced cementite decomposition in pearlite. Acta Materialia, 2011, 59, 3965-3977.	3.8	269
5	Segregation engineering enables nanoscale martensite to austenite phase transformation at grain boundaries: A pathway to ductile martensite. Acta Materialia, 2013, 61, 6132-6152.	3.8	264
6	Chemical gradients across phase boundaries between martensite and austenite in steel studied by atom probe tomography and simulation. Acta Materialia, 2011, 59, 364-374.	3.8	255
7	Segregation Stabilizes Nanocrystalline Bulk Steel with Near Theoretical Strength. Physical Review Letters, 2014, 113, 106104.	2.9	224
8	Precipitation and austenite reversion behavior of a maraging steel produced by selective laser melting. Journal of Materials Research, 2014, 29, 2072-2079.	1.2	221
9	Microstructural evolution of a Ni-based superalloy (617B) at 700°C studied by electron microscopy and atom probe tomography. Acta Materialia, 2012, 60, 1731-1740.	3.8	212
10	Atomic-scale analysis of carbon partitioning between martensite and austenite by atom probe tomography and correlative transmission electron microscopy. Acta Materialia, 2014, 65, 215-228.	3.8	205
11	Evolution of strength and microstructure during annealing of heavily cold-drawn 6.3 GPa hypereutectoid pearlitic steel wire. Acta Materialia, 2012, 60, 4005-4016.	3.8	187
12	Metallic composites processed via extreme deformation: Toward the limits of strength in bulk materials. MRS Bulletin, 2010, 35, 982-991.	1.7	180
13	Elemental partitioning and mechanical properties of Ti- and Ta-containing Co–Al–W-base superalloys studied by atom probe tomography and nanoindentation. Acta Materialia, 2014, 78, 78-85.	3.8	168
14	Nanoscale austenite reversion through partitioning, segregation and kinetic freezing: Example of a ductile 2GPa Fe–Cr–C steel. Acta Materialia, 2012, 60, 2790-2804.	3.8	167
15	Atomic-scale compositional characterization of a nanocrystalline AlCrCuFeNiZn high-entropy alloy using atom probe tomography. Acta Materialia, 2013, 61, 4696-4706.	3.8	138
16	Element-Resolved Corrosion Analysis of Stainless-Type Glass-Forming Steels. Science, 2013, 341, 372-376.	6.0	136
17	Dynamic strain aging studied at the atomic scale. Acta Materialia, 2015, 86, 34-42.	3.8	136
18	Thermal stability of electrodeposited nanocrystalline Co-1.1at.%P. Acta Materialia, 2005, 53, 4473-4481.	3.8	135

#	Article	IF	CITATIONS
19	Advanced Scale Bridging Microstructure Analysis of Single Crystal Niâ€Base Superalloys. Advanced Engineering Materials, 2015, 17, 216-230.	1.6	117
20	Enhanced Congo red dye removal from aqueous solutions using iron nanoparticles: adsorption, kinetics, and equilibrium studies. Dalton Transactions, 2017, 46, 15470-15479.	1.6	103
21	Atomically Embedded Ag via Electrodiffusion Boosts Oxygen Evolution of CoOOH Nanosheet Arrays. ACS Catalysis, 2020, 10, 562-569.	5.5	93
22	Investigation of the diffusion behavior of sodium in Cu(In,Ga)Se2 layers. Journal of Applied Physics, 2014, 115, .	1.1	90
23	Characterization of Grain Boundaries in Cu(In,Ga)Se\$_{f 2}\$ Films Using Atom-Probe Tomography. IEEE Journal of Photovoltaics, 2011, 1, 207-212.	1.5	87
24	Confined and Chemically Flexible Grain Boundaries in Polycrystalline Compound Semiconductors. Advanced Energy Materials, 2012, 2, 992-998.	10.2	84
25	Interface-directed spinodal decomposition in TiAlN/CrN multilayer hard coatings studied by atom probe tomography. Acta Materialia, 2013, 61, 7534-7542.	3.8	77
26	Shear-Induced Mixing Governs Codeformation of Crystalline-Amorphous Nanolaminates. Physical Review Letters, 2014, 113, 035501.	2.9	70
27	Shear band-driven precipitate dispersion for ultrastrong ductile medium-entropy alloys. Nature Communications, 2021, 12, 4703.	5.8	70
28	On the Spheroidized Carbide Dissolution and Elemental Partitioning in High Carbon Bearing Steel 100Cr6. Metallurgical and Materials Transactions A: Physical Metallurgy and Materials Science, 2014, 45, 595-606.	1.1	60
29	Effects of phase composition and elemental partitioning on soft magnetic properties of AlFeCoCrMn high entropy alloys. Acta Materialia, 2019, 171, 31-39.	3.8	60
30	Comparative atom probe study of Cu(In,Ga)Se2 thin-film solar cells deposited on soda-lime glass and mild steel substrates. Journal of Applied Physics, 2011, 110, .	1.1	59
31	On the detection of multiple events in atom probe tomography. Ultramicroscopy, 2018, 189, 54-60.	0.8	59
32	(Nb _{<i>x</i>} , Zr _{1–<i>x</i>}) ₄ AlC ₃ MAX Phase Solid Solutions: Processing, Mechanical Properties, and Density Functional Theory Calculations. Inorganic Chemistry, 2016, 55, 5445-5452.	1.9	54
33	A new method for mapping the three-dimensional atomic distribution within nanoparticles by atom probe tomography (APT). Ultramicroscopy, 2018, 190, 30-38.	0.8	51
34	Cuâ€Rich Precursors Improve Kesterite Solar Cells. Advanced Energy Materials, 2014, 4, 1300543.	10.2	49
35	Effects of Ru on elemental partitioning and precipitation of topologically close-packed phases in Ni-based superalloys. Scripta Materialia, 2015, 101, 44-47.	2.6	49
36	The Maximum Separation Cluster Analysis Algorithm for Atom-Probe Tomography: Parameter Determination and Accuracy. Microscopy and Microanalysis, 2014, 20, 1662-1671.	0.2	46

#	Article	IF	CITATIONS
37	Crucial microstructural feature to determine the impact toughness of intercritically annealed medium-Mn steel with triplex-phase microstructure. Acta Materialia, 2019, 164, 122-134.	3.8	46
38	Enhancement of the photocatalytic reactivity of TiO2 nano-particles by a simple mechanical blending with hydrophobic mordenite (MOR) zeolite. Applied Catalysis B: Environmental, 2009, 89, 406-410.	10.8	44
39	Elemental partitioning and site-occupancy in γ/γ′ forming Co-Ti-Mo and Co-Ti-Cr alloys. Scripta Materialia, 2018, 154, 159-162.	2.6	44
40	Atomic cale Mapping of Impurities in Partially Reduced Hollow TiO ₂ Nanowires. Angewandte Chemie - International Edition, 2020, 59, 5651-5655.	7.2	42
41	Passivation of Deep-Level Defects by Cesium Fluoride Post-Deposition Treatment for Improved Device Performance of Cu(In,Ga)Se ₂ Solar Cells. ACS Applied Materials & Interfaces, 2019, 11, 35653-35660.	4.0	41
42	On Local Phase Equilibria and the Appearance of Nanoparticles in the Microstructure of Single rystal Niâ€Base Superalloys. Advanced Engineering Materials, 2016, 18, 1556-1567.	1.6	39
43	Dissecting functional degradation in NiTi shape memory alloys containing amorphous regions via atomistic simulations. Acta Materialia, 2021, 202, 331-349.	3.8	39
44	Reducing Time to Discovery: Materials and Molecular Modeling, Imaging, Informatics, and Integration. ACS Nano, 2021, 15, 3971-3995.	7.3	36
45	Mechanisms of extrinsic alkali incorporation in CIGS solar cells on flexible polyimide elucidated by nanoscale and quantitative analyses. Nano Energy, 2020, 67, 104201.	8.2	35
46	Orientation-dependent plastic deformation mechanisms and competition with stress-induced phase transformation in microscale NiTi. Acta Materialia, 2021, 208, 116731.	3.8	31
47	On the nature of twin boundary-associated strengthening in Fe-Mn-C steel. Scripta Materialia, 2018, 156, 27-31.	2.6	30
48	Thermal stability of TiAlN/CrN multilayer coatings studied by atom probe tomography. Ultramicroscopy, 2011, 111, 518-523.	0.8	29
49	Self-assembled nano-composite perovskites as highly efficient and robust hybrid cathodes for solid oxide fuel cells. Journal of Materials Chemistry A, 2022, 10, 2496-2508.	5.2	29
50	Improved strength of a medium-Mn steel by V addition without sacrificing ductility. Materials Science & Engineering A: Structural Materials: Properties, Microstructure and Processing, 2021, 802, 140681.	2.6	27
51	On the microstructural evolution and partitioning behavior of L12-structured γ′-based Co-Ti-W alloys upon Cr and Al alloying. Intermetallics, 2019, 104, 97-102.	1.8	26
52	Interaction of tungsten nanopowders with air under different conditions. Scripta Materialia, 2005, 52, 375-380.	2.6	24
53	Thermal dissolution mechanisms of AlN/CrN hard coating superlattices studied by atom probe tomography and transmission electron microscopy. Acta Materialia, 2015, 85, 32-41.	3.8	24
54	Unraveling the Metastability of C _{<i>n</i>} ²⁺ (<i>n</i> = 2–4) Clusters. Journal of Physical Chemistry Letters, 2019, 10, 581-588.	2.1	24

#	Article	IF	CITATIONS
55	Modulation of plastic flow in metallic glasses via nanoscale networks of chemical heterogeneities. Acta Materialia, 2017, 140, 116-129.	3.8	21
56	Application of Focused Ion Beam to Atom Probe Tomography Specimen Preparation from Mechanically Alloyed Powders. Microscopy and Microanalysis, 2007, 13, 347-353.	0.2	19
57	Deformation induced alloying in crystalline – metallic glass nano-composites. Materials Science & Engineering A: Structural Materials: Properties, Microstructure and Processing, 2015, 628, 269-280.	2.6	19
58	Evaluation of Analysis Conditions for Laser-Pulsed Atom Probe Tomography: Example of Cemented Tungsten Carbide. Microscopy and Microanalysis, 2017, 23, 431-442.	0.2	19
59	A simple and robust route toward flexible CIGS photovoltaic devices on polymer substrates: Atomic level microstructural analysis and local opto-electronic investigation. Solar Energy Materials and Solar Cells, 2019, 195, 280-290.	3.0	19
60	Tailoring nanostructured NbCoSn-based thermoelectric materials via crystallization of an amorphous precursor. Nano Energy, 2021, 80, 105518.	8.2	19
61	Atom Probe Tomography Studies on the Cu(In,Ga)Se ₂ Grain Boundaries. Journal of Visualized Experiments, 2013, , .	0.2	18
62	Atomic diffusion induced degradation in bimetallic layer coated cemented tungsten carbide. Corrosion Science, 2017, 120, 1-13.	3.0	18
63	Compositional gradients and impurity distributions in CuInSe ₂ thinâ€film solar cells studied by atom probe tomography. Surface and Interface Analysis, 2012, 44, 1386-1388.	0.8	17
64	Fabrication of Atom Probe Tomography Specimens from Nanoparticles Using a Fusible Bi–In–Sn Alloy as an Embedding Medium. Microscopy and Microanalysis, 2019, 25, 438-446.	0.2	17
65	Effects of Mo on the mechanical behavior of γ/γʹ-strengthened Co-Ti-based alloys. Acta Materialia, 2020, 197, 69-80.	3.8	16
66	Three-dimensional atomic mapping of ligands on palladium nanoparticles by atom probe tomography. Nature Communications, 2021, 12, 4301.	5.8	16
67	Spallation resistance of oxide scales on Alloy 617 enhanced by boron addition. Corrosion Science, 2018, 140, 196-204.	3.0	14
68	FeNiCoAlTaB superelastic and shape-memory wires with oligocrystalline grain structure. Scripta Materialia, 2020, 188, 1-5.	2.6	13
69	On the oxygen-induced hot cracking in a direct laser deposited Ni-based superalloy. Scripta Materialia, 2021, 196, 113751.	2.6	13
70	Stabilization of monodispersed spherical silica particles and their alignment with reduced crack density. Colloids and Surfaces A: Physicochemical and Engineering Aspects, 2014, 441, 354-359.	2.3	12
71	On the Multiple Event Detection in Atom Probe Tomography. Microscopy and Microanalysis, 2017, 23, 618-619.	0.2	12
72	Characterization of Pd and Pd@Au core-shell nanoparticles using atom probe tomography and field evaporation simulation. Journal of Alloys and Compounds, 2020, 831, 154721.	2.8	12

#	Article	IF	CITATIONS
73	Hot cracking behavior of additively manufactured D2 steel. Materials Characterization, 2021, 178, 111217.	1.9	11
74	Transmission electron microscopy and atom probe specimen preparation from mechanically alloyed powder using the focused ion-beam lift-out technique. Journal of Electron Microscopy, 2007, 56, 43-49.	0.9	10
75	Additive manufacturing of titanium-base alloys with equiaxed microstructures using powder blends. Additive Manufacturing, 2020, 36, 101467.	1.7	10
76	Homogeneity of mechanically alloyed nano-crystalline Fe – Cu-powders. International Journal of Materials Research, 2008, 99, 541-547.	0.1	8
77	Oxidation behavior of AlN/CrN multilayered hard coatings. Nano Convergence, 2017, 4, 15.	6.3	8
78	Compositional evolution of long-period stacking ordered structures in magnesium studied by atom probe tomography. Scripta Materialia, 2018, 156, 55-59.	2.6	8
79	Investigation of sputter-deposited Al–2at.%Cu layers by means of the tomographic atom probe (TAP). Scripta Materialia, 2005, 53, 323-327.	2.6	7
80	Publisher's Note: Shear-Induced Mixing Governs Codeformation of Crystalline-Amorphous Nanolaminates [Phys. Rev. Lett. 113 , 035501 (2014)]. Physical Review Letters, 2014, 113, .	2.9	7
81	Microstructural evolution of the heat affected zone of a Co–Ti–W alloy upon laser cladding with a CoNiCrAlY coating. Materials Characterization, 2019, 158, 109998.	1.9	7
82	Enhanced microstructural stability of γ/γ′-strengthened Co-Ti-Mo-based alloys through Al additions. Acta Materialia, 2021, 214, 117011.	3.8	7
83	An assessment of the homogeneity of nano-crystalline Fe–Cu powders as studied by means of APT. Ultramicroscopy, 2009, 109, 599-605.	0.8	6
84	Detection of Cu2Zn5SnSe8 and Cu2Zn6SnSe9 phases in co-evaporated Cu2ZnSnSe4 thin-films. Applied Physics Letters, 2015, 107, .	1.5	6
85	Amorphous phase separation in an Fe-based bulk metallic glass. Materials Letters, 2017, 190, 161-164.	1.3	6
86	Nano-scale Characterization of Thin-Film Solar Cells. Microscopy and Microanalysis, 2014, 20, 394-395.	0.2	5
87	Effects of transformation-induced plasticity on the small-scale deformation behavior of single crystalline complex concentrated alloys. Scripta Materialia, 2020, 176, 122-125. Variable chemical decoration of extended defects in Cu-poor <mml:math< td=""><td>2.6</td><td>5</td></mml:math<>	2.6	5
88	xmlns:mml="http://www.w3.org/1998/Math/MathML"> <mml:mrow> <mml:mi mathvariant="normal">C <mml:msub> <mml:mi mathvariant="normal">u <mml:mn>2 </mml:mn> </mml:mi </mml:msub> <mml:mi>ZnSnS </mml:mi> <mml:msub> mathvariant="normal">e <mml:mn>4 </mml:mn> </mml:msub> </mml:mi </mml:mrow> thin	< <mark>0.9</mark> <mml:mi< td=""><td>5</td></mml:mi<>	5
89	films. Physical Review Materials, 2019, 3, Atom Probe Tomography Investigations of Ag Nanoparticles Embedded in Pulse-Electrodeposited Ni Films. Microscopy and Microanalysis, 2021, 27, 1007-1016.	0.2	4
90	Formation of nanometer-sized Cu-Sn-Se particles in Cu2ZnSnSe4 thin-films and their effect on solar cell efficiency. Acta Materialia, 2017, 132, 276-284.	3.8	3

#	Article	IF	CITATIONS
91	Decomposition behavior of yttria-stabilized zirconia and its effect on directed energy deposited Ti-based composite material. Journal of Materials Science and Technology, 2022, 112, 138-150.	5.6	3
92	Kinetic stabilization of a topotactically transformed texture morphology <i>via</i> doping in Ni-rich lithium layered oxides. Journal of Materials Chemistry A, 2022, 10, 13735-13743.	5.2	3
93	Co-deformation of crystalline-amorphous nanolaminates. Microscopy and Microanalysis, 2015, 21, 361-362.	0.2	2
94	Degradation Mechanism of Molds for Precision Glass Molding. Microscopy and Microanalysis, 2017, 23, 698-699.	0.2	1
95	Spatial Distributions of Alloying Elements Obtained from Atom Probe Tomography of the Amorphous Ribbon Fe75C11Si2B8Cr4. Korean Journal of Materials Research, 2013, 23, 190-193.	0.1	1
96	Elemental Sub-Lattice Occupation and Microstructural Evolution in γ/γ′ Co–12Ti–4Mo–Cr Alloys. Microscopy and Microanalysis, 2021, , 1-5.	0.2	0
97	Atom Probe Tomography: Unveiling the Elemental Distribution in Nanostructured Materials With Near-Atomic Resolution. , 2022, , 641-647.		0
98	Atom Probe Tomography: A Characterization Method for Three-dimensional Elemental Mapping at the Atomic Scale. Journal of Korean Powder Metallurgy Institute, 2012, 19, 67-71.	0.2	0
99	Novel approaches for analyzing nanoparticles using Atom Probe Tomography. Journal of Surface Analysis (Online), 2019, 26, 140-141.	0.1	0
100	Joining dissimilar metal of Ti and CoCrMo using directed energy deposition. Journal of Materials Science and Technology, 2021, 111, 99-99.	5.6	0